

## Origin of green emission and charge trapping dynamics in ZnO nanowires

Mingjie Li,<sup>1</sup> Guichuan Xing,<sup>1,2,3</sup> Guozhong Xing,<sup>4</sup> Bo Wu,<sup>1</sup> Tom Wu,<sup>1</sup> Xinhai Zhang,<sup>5</sup> and Tze Chien Sum<sup>1,2,3,\*</sup>

<sup>1</sup>*Division of Physics and Applied Physics, School of Physical and Mathematical Sciences, Nanyang Technological University, 21 Nanyang Link, Singapore 637371*

<sup>2</sup>*Energy Research Institute @ NTU (ERI@N), Nanyang Technological University, 50 Nanyang Drive, Singapore 637553*

<sup>3</sup>*Singapore-Berkeley Research Initiative for Sustainable Energy (SinBeRISE), 1 Create Way, Singapore 138602*

<sup>4</sup>*School of Materials Science and Engineering, The University of New South Wales, Sydney, New South Wales 2052, Australia*

<sup>5</sup>*Institute of Materials Research and Engineering, A\*STAR (Agency for Science, Technology and Research), 3 Research Link, Singapore 117602, Singapore*

(Received 19 November 2012; revised manuscript received 1 February 2013; published 18 March 2013)

The origins of the commonly observed green emission (GE) from ZnO nanostructures remain highly controversial despite extensive studies over the past few decades. Herein, through a comprehensive ultrafast optical spectroscopy study, new insights into its origin and the charge trapping dynamics at the GE centers in ZnO nanowires prepared by the vapor transport method are gained. Transient absorption spectroscopy (TAS) revealed a sub-band-gap absorption bleaching band arising from the state filling of the electrons in the conduction band and holes trapped in the GE centers. The GE originates from the recombination between the electrons in the conduction band and/or shallow donor levels and the holes trapped at the GE centers (which are located at  $\sim 0.88$  eV above the valence band). Importantly, an ultrafast excitonic Auger-type hole trapping process to the GE centers occurring in a subpicosecond time scale was also uncovered by TAS—shedding new light on the mechanism behind the fast and efficient charge trapping of photoexcited carriers. The knowledge gained is crucial for the development of ZnO-based optoelectronic devices.

DOI: [10.1103/PhysRevB.87.115309](https://doi.org/10.1103/PhysRevB.87.115309)

PACS number(s): 78.47.J–, 82.53.Mj

### I. INTRODUCTION

Zinc oxide (ZnO), a wide-band-gap semiconductor ( $E_g = 3.37$  eV at 298 K), is one of the most important functional materials today due to its diverse morphology, physiochemical properties, and wide applications.<sup>1</sup> Typically, ZnO nanostructures exhibit a band-edge emission (BE) in the near-UV region and a defect-related emission occurring in the visible region due to the different kinds of defects in the materials. Recent studies have shown that the defects in semiconductor nanostructures play a crucial role in enhancing the performance of photovoltaic and photocatalytic devices.<sup>2–4</sup> For example, enhanced photocatalytic activity was reported in ZnO nanostructures with high green emission (GE) intensities though its exact enhancement mechanism remains unclear.<sup>5–7</sup> Hence, a deep understanding of the origin of the defect-related emission and the role of defects on the charge carrier trapping/separation (following photoexcitation) is key to optimizing the performance of ZnO-based nanoscale devices.

The wide range of visible emissions in ZnO nanostructures is due to the different kinds of defects depending on the fabrication method/conditions. For instance, ZnO nanostructures prepared by low-temperature wet-chemical methods typically yield a green to yellow emission (peaking from 520 to 650 nm)—attributed to the deep subsurface defects (e.g., oxygen vacancy, Li doping, or zinc interstitial).<sup>8–11</sup> Specifically, a broad GE band centered around 500–515 nm (over a narrower range of wavelengths) is commonly observed in ZnO nanostructures prepared by the high-temperature vapor-phase transport (VPT) method<sup>12–14</sup>—attributed to the on/near surface defects.<sup>14–17</sup> Despite the extensive studies on the GE in ZnO, there is still no consensus on its origin. Proposed origins include: (a) extrinsic Cu impurities<sup>18</sup> and (b) intrinsic defects

such as oxygen vacancy ( $V_O$ ),<sup>19,20</sup> zinc vacancy ( $V_{Zn}$ ),<sup>21</sup> oxygen antisite ( $O_{Zn}$ ),<sup>22</sup> and Zn interstitial ( $Zn_i$ ),<sup>23,24</sup> or their complexes.<sup>14,25</sup> Among the above-mentioned intrinsic point defects, both  $V_O$  and  $V_{Zn}$  are commonly believed to be the source of the GE in ZnO. For  $V_O$ , it was proposed that the GE originates from the recombination of electrons in the singly ionized oxygen vacancy ( $V_O^+$ ) with the photoexcited holes in the valence band (VB).<sup>19</sup> Nevertheless, anticorrelations between the occurrence of the GE and the electron paramagnetic resonance (EPR) signals from  $V_O$  in ZnO tetrapods<sup>14</sup> and also that between the occurrence of the GE and the concentration of  $V_O$  from x-ray photoemission spectroscopy (XPS) measurements<sup>26</sup> in our  $H_2$ -annealed ZnO nanowires (NWs) suggest otherwise. Recently, it was suggested that  $V_O^+$  gives rise to the red emission of  $\sim 1.89$  eV according to EPR measurements.<sup>27</sup> Next,  $V_{Zn}$  was also proposed as a likely source of the GE given that  $V_{Zn}$  has a calculated  $\varepsilon(-/2-)$  transition level of  $\sim 0.9$  eV above the valence band maximum (VBM).<sup>21</sup> However, recent EPR and optically detected magnetic resonance (ODMR) revealed that the isolated  $V_{Zn}$  defect in bulk single crystals had a red emission of  $\sim 1.6$  eV with a large Stokes shift of  $\sim 0.8$  eV.<sup>28</sup> Furthermore, it was also reported that isolated  $V_{Zn}$  from ZnO thin films exhibit a red emission with a lifetime of  $\sim 1$ –4 ns,<sup>29</sup> thereby casting further doubt on  $V_{Zn}$  as a contender for GE. Apart from point defects, defect complexes were also proposed as one of the candidates for GE. Recent density functional theory (DFT) calculations considered  $V_O + V_{Zn}$  divacancies ( $V_{ZnO}$ ) (i.e., missing a Zn-O dimer) as a possible origin of the GE.<sup>25</sup> It was calculated that the  $\varepsilon(q/q+1)$  charge transition of  $V_{ZnO}$  is located at about 2.2–2.5 eV below the conduction band minimum (CBM) and possesses a small lattice relaxation energy in the range of

70–120 meV. The  $V_{\text{ZnO}}$  origin of the GE is further supported by another DFT study, which had also calculated the  $\varepsilon(+/0)$  transition level of  $V_{\text{ZnO}}$  to be located at  $\sim 0.6\text{--}0.8$  eV above the VBM<sup>30</sup>—the electron transition from the conduction band (CB) to  $V_{\text{ZnO}}$  would result in the GE ( $\sim 2.5$  eV). Furthermore,  $V_{\text{ZnO}}$  is also predicted to be the predominant defect type on the nonpolar  $(10\bar{1}0)$  surface of ZnO instead of  $V_{\text{O}}$ .<sup>31</sup> As the GE is believed to originate from the surface defects,<sup>14–16</sup>  $V_{\text{ZnO}}$  could therefore be a prime suspect.

Ultrafast optical spectroscopy (UOS) techniques such as femtosecond transient absorption spectroscopy (TAS) and time-resolved photoluminescence (TRPL) are powerful probes of carrier dynamics in semiconductor nanostructures.<sup>32</sup> For ZnO nanostructures, the dynamics and the mechanism of carrier trapping to the intrinsic defects have rarely been investigated in depth. Elucidating the origin of the GE in unintentionally doped (undoped) ZnO nanowires (NWs) prepared by the VPT method and its charge trapping dynamics using UOS techniques are the main foci of this paper. This was performed in a comparative study involving as-grown, air-annealed, and  $\text{H}_2$ -annealed ZnO samples. Importantly, TAS revealed an ultrafast subpicosecond (sub-ps) excitonic Auger-type hole trapping to the GE centers that permits the fast and efficient charge trapping/separation in these NWs. This could account for the enhanced photocatalytic activity reported in ZnO nanostructures.<sup>5–7</sup> Our findings therefore have important implications for the development of high-efficiency ZnO-based photovoltaic and photocatalytic devices.

## II. EXPERIMENT DETAILS

*ZnO NWs synthesis.* Vertically aligned ZnO NWs were grown on *c*-plane sapphire substrate by the vapor transport method. Briefly, a mixture of ZnO powder (99.999%, Aldrich) and graphite powder (99.999%, Aldrich) with a weight ratio of 1:1 was used as the source. After coating a thin layer (1–2 nm) of Au on the substrate as a catalyst, the substrate was placed in a quartz tube. The temperature was slowly raised and kept at about 850 °C for 15 min for NW growth. High-purity argon mixed with 5% oxygen with a constant flow rate of 50 SCCM (SCCM denotes cubic centimeter per minute at STP) was used as the carrying gas. The as-grown sample was then divided into three pieces: One piece was kept without any further treatment—*as-grown*; one piece was annealed in air (at atmospheric pressure) at 600 °C for 30 min—*air-annealed*, and another piece was annealed in forming gas (90% Ar + 10%  $\text{H}_2$ ,  $\text{H}_2$  pressure: 25 mbar) at 420 °C for 30 min— *$\text{H}_2$ -annealed*.

*Time-integrated and time-resolved PL spectroscopy.* The samples were excited using 325-nm UV excitation pulses (with pulse duration of  $< 150$  fs) generated from a Coherent TOPAS-C optical parametric amplifier (OPA) that was pumped by a 1 kHz Coherent Legend Ti:sapphire regenerative amplifier, which in turn was seeded by a 80 MHz Coherent Vitesse oscillator. The time-integrated photoluminescence (TIPL) spectra were collected in a conventional backscattering geometry and detected by a charge-coupled device array (Princeton Instruments, Pixis 400B) coupled to a monochromator (Acton, Spectra Pro 2500i). The temporal evolution of the PL was recorded by an Optronis Optoscope streak camera system in TRPL measurements, which has an ultimate system temporal

resolution of 10 ps when operated in the shortest time window of 330 ps.

*UV-pump/white-light-probe spectroscopy.* Differential transmission ( $\Delta T/T$ ) spectra of ZnO NWs were performed in a nondegenerate pump-probe configuration with chirp correction, where  $\Delta T/T = (T - T_0)/T_0$  (where  $T_0$  is the transmission of probe beam without pump excitation of the sample,  $T$  is transmission of probe beam with pump excitation of the sample). The 350-nm pump pulses were focused onto a 200- $\mu\text{m}$  spot and overlapped with white-light continuum probe pulses generated with a thin sapphire plate (that was focused by a parabolic mirror to a spot of  $\sim 20$   $\mu\text{m}$  diameter). The direction of the probe pulse is perpendicular to the substrate and parallel with the NWs growth direction. Pump-induced changes were monitored using a monochromator/photomultiplier tube (PMT) configuration coupled to a lock-in amplifier. The pump beam was chopped at 83 Hz and used as the reference frequency for the lock-in. The system response was determined by the two-photon absorption cross correlation between pump and probe pulses in ZnO for 500 nm.

## III. RESULTS AND DISCUSSION

### A. Sample characterization

Figure 1(a) shows a representative scanning electron microscope (SEM) image of the uniformly distributed, vertically aligned as-grown ZnO NWs with diameters ranging from 80 to 100 nm and lengths of  $\sim 1$   $\mu\text{m}$  grown on a sapphire substrate by the VPT method.<sup>33</sup> The NWs are grown along the  $[0001]$  direction and are enclosed by  $(10\bar{1}0)$  facets with a wurtzite structure—consistent with the previous results of ZnO

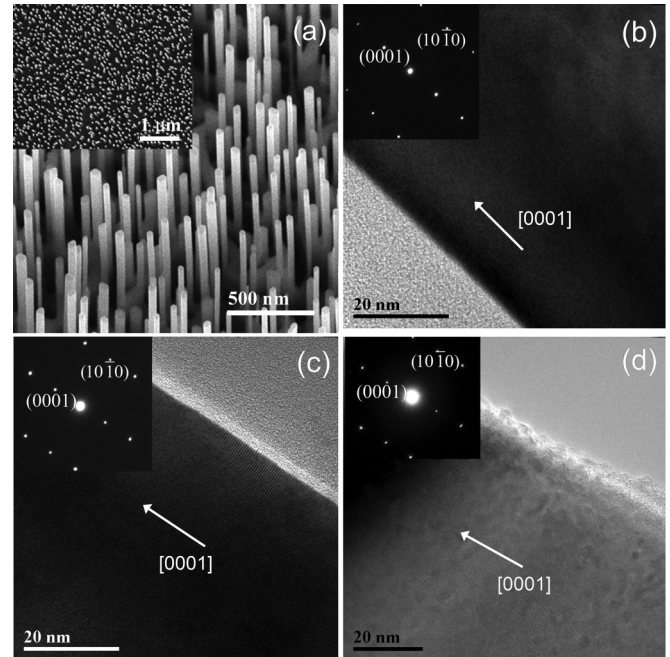


FIG. 1. (a) SEM image of the as-grown ZnO NWs. Inset shows the top view of the NWs. Transmission electron microscopy (TEM) images and selected-area electron diffraction (SAED) patterns of the (b) as-grown, (c) air-annealed, and (d)  $\text{H}_2$ -annealed ZnO NWs.

NWs prepared by the same method.<sup>7,15</sup> Postfabrication thermal annealing of the as-grown samples under oxidizing/reducing ambient was used to modulate the concentration of GE centers. The structural form of the NWs was not severely altered after the postfabrication annealing [Figs. 1(c) and 1(d)] though the H<sub>2</sub>-annealed samples were found to have a roughened polycrystalline surface with small ZnO particulates (under TEM) and some NWs are bundled together after air annealing (see Supplemental Material<sup>34</sup>).

### B. Mechanism of GE in undoped ZnO NWs

Figure 2(a) shows the room-temperature (RT) PL spectra for the as-grown, air-annealed, and H<sub>2</sub>-annealed ZnO samples. All three samples exhibit a strong BE peak at around 378 nm (3.28 eV) and a broad GE band peaking at 505 nm (2.46 eV). Apart from the GE intensity variation, similarities in the GE spectral shape among the three samples indicate that the GE originates from a common origin. The BE becomes quenched while the GE band becomes enhanced after air-annealing—consistent with the previous reports for oxygen-annealed, VPT-grown ZnO NWs.<sup>35,36</sup> The decrease of BE should be due to the increased defects which act as trapping centers for the photoexcited carriers. The increase in the GE intensity after air annealing can be tentatively attributed to the increased concentration of  $V_{ZnO}$ , this assumption is supported by the findings that  $V_{ZnO}$  has lower formation energy on the nonpolar (10 $\bar{1}0$ ) surfaces and is preferentially formed during the air annealing and the subsequent cooling to RT.<sup>31</sup> The decrease in the GE intensity following hydrogenation is also commonly observed in ZnO nanostructures prepared by the same method,<sup>37</sup> and this is attributed to the passivation of the acceptor-like defects by the formation of hydrogen-related defects complex (e.g.,  $V_{Zn}-H_2$ ).<sup>38</sup>

The structured peaks separated by the energy of longitudinal optical phonon in GE (peaking at  $\sim 2.43$  eV) at low temperatures (LT), commonly seen in VPT-grown ZnO nanostructures,<sup>14,17</sup> are observed in the undoped ZnO NWs [Figs. 2(b) and 2(c)]. This structured GE was previously suggested to originate from the Cu dopant at the Zn site (i.e.,  $Cu_{Zn}$ ). However, subsequent EPR studies showed a null signal for Cu ions in undoped ZnO tetrapods (prepared by vapor transport method)<sup>14</sup> despite exhibiting a structured GE band at LT. It was also found that the intensity and/or the position of the GE were dependent on the fabrication gas and the annealing conditions, indicating that the GE centers were more likely intrinsic defects.<sup>14</sup> Furthermore, similar fine structures were also observed in the deep-level emissions at LT in many undoped wide-band-gap semiconductors, such as the blue and yellow emission band in GaN,<sup>39–41</sup> yellow emission in ZnO thin film,<sup>42</sup> and green emission in In<sub>2</sub>O<sub>3</sub> NWs.<sup>43</sup> In view of these reports, observation of a structured GE band in undoped ZnO at LT may not be a key indication of the GE originating from Cu impurities. This argument is strongly supported by the distinct PL transients exhibited by the undoped ZnO NWs and (intentionally) Cu-doped ZnO NWs from our detailed TRPL studies (see Fig. S2 and discussion in the Supplemental Material<sup>34</sup>). Hence, we believe that this structured GE in undoped ZnO NWs arises from the transitions between shallow donors and a deep acceptor level—described in a vibronic

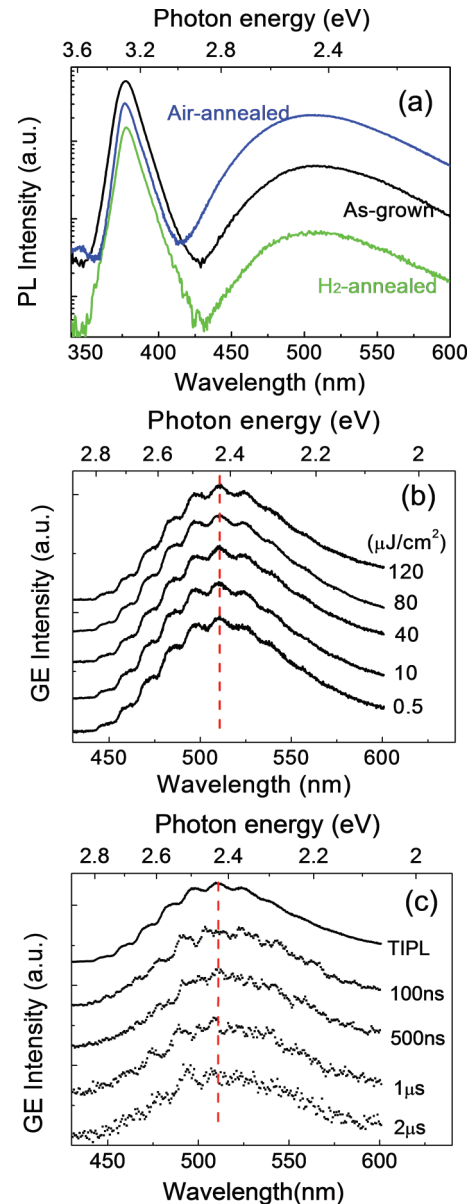


FIG. 2. (Color online) (a) RT time-integrated PL spectra plotted on a semilog scale for the as-grown (black), air-annealed (blue), and H<sub>2</sub>-annealed (green) ZnO NWs with an excitation fluence of 50  $\mu\text{J}/\text{cm}^2$ ; (b) a comparison of the normalized pump-fluence-dependent TIPL spectra of the GE band (for the air-annealed ZnO NWs) with increasing pump fluence at 10 K. The dashed red line at the peak of the GE band is a guide to the eye; (c) comparison of the TIPL spectrum (solid line) of the GE with the temporal evolution of the GE band at various times following photoexcitation of the air-annealed ZnO NWs at 10 K. Note that the PL intensities are normalized and the excitation fluence used was 50  $\mu\text{J}/\text{cm}^2$ .

model.<sup>44</sup> Lastly, we also wish to emphasize that the growth temperature of these ZnO NWs also has a strong influence on their emission properties. These undoped samples in this study were fabricated at a temperature of  $\sim 850^\circ\text{C}$  while those undoped ZnO NWs used as a control in the earlier charge transfer study of Cu-doped ZnO NWs were fabricated at a temperature of  $\sim 960^\circ\text{C}$  (experimental details for the growth of Cu-doped ZnO NWs can be found in Ref. 45). The latter

undoped ZnO NWs possess a very weak GE band in relation to its BE.<sup>45</sup>

Next, we shall examine the recombination mechanism at the GE centers. The GE lifetime is relatively long ( $\sim\mu\text{s}$ ) as evident from the TRPL decay transients shown in Fig. S2(c) in Ref. 34. Therefore, we expect that carrier trapping to these centers will be fast; otherwise, carrier recombination via the BE (with sub-ns lifetimes) will be favored and the GE will be greatly suppressed. Figure 2(b) shows the normalized pump-fluence-dependent GE spectra from the representative air-annealed sample at 10 K. The GE band (peaking at  $\sim 2.43$  eV) remains relatively invariant with negligible spectra shift as the pump fluence increases—which is consistent for all the other samples as well. Similar behavior is also observed for measurements at RT. Figure 2(c) shows the temporal evolution of the GE band from the same air-annealed sample obtained at different times. There is no noticeable spectral/energy shift of the GE band at various times compared to the TIPL spectrum within an experimental accuracy of  $<10$  meV. Similar results had also been reported for the yellow emission in GaN.<sup>46</sup> The absence of an energy shift of the GE with increasing pump excitation or increasing temporal delay rules out the possibility of donor-acceptor pair (DAP) recombination between the localized donors and acceptors. Such recombination would result in key spectral and temporal signatures of (i) blue shift of the emission spectra with increased pump excitation as the closer DAPs become excited, and (ii) red shift of the emission peaks as the closer pairs recombine faster since the recombination rate is dependent on the distance between the donor and acceptor. However, DAP involving shallow (delocalized) donors or acceptors would induce very small shifts (of a few meV).<sup>47,48</sup> It was reported that shallow acceptors arising from the stacking effect yield a PL band at around 3.31 eV in ZnO at LT.<sup>49</sup> However, the absence of such peak near 3.31 eV in the LT PL spectrum rules out the possibility of these shallow acceptors in our samples (see Fig. S3 in the Supplemental Material<sup>34</sup>). Thus, the GE involves the transitions of the free electrons in the CB and/or those electrons trapped at shallow (delocalized) donor levels with holes trapped at the deep levels (i.e., GE centers) as proposed in Fig. 4(b).

### C. State filling of the GE centers

To validate the hypothesis of fast carrier trapping to the GE centers, TAS was used to probe the carrier trapping dynamics. Femtosecond TAS with UV-pump/sub-band-gap probe differential transmission (DT or  $\Delta T/T$ ) measurements (with the pump/probe beams aligned nearly parallel to the vertically aligned NWs) was performed.

Figure 3(a) shows the linear absorption spectra and the GE band in the representative air-annealed sample. However, due to the strong light scattering by the NW ensemble, transitions involving the defect states in the band gap could not be resolved in the linear absorption spectrum. Figure 3(b) shows the DT spectra at a time delay of 2 ps following 350-nm photoexcitation. The photobleaching (PB) band (i.e., positive  $\Delta T/T$  signals) centered at about 470 nm (or 2.64 eV) is present in all three samples. Previously, an increase of pump-induced absorption of visible light was observed in ZnO nanoparticles

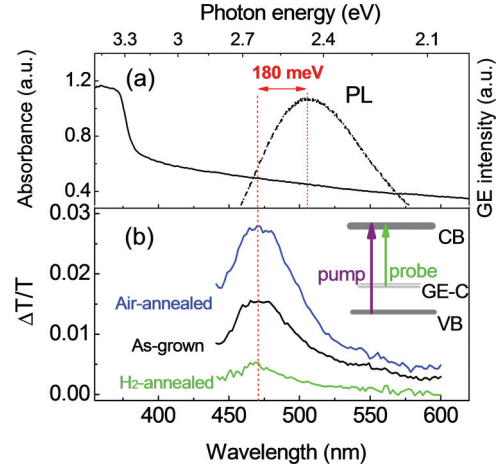


FIG. 3. (Color online) (a) Linear absorption spectra (solid) and the GE band (dashed) of the air-annealed ZnO NWs; (b) DT spectra taken at 2 ps after excitation ( $T = 300$  K) for the different samples. Inset shows a schematic of the energy levels excited and probed in the pump-probe measurement: (CB) conduction band; (VB) valence band; (GE-C) GE centers.

(NPs) (prepared by wet-chemical methods)—attributed to the absorption of the probe beam by the photoexcited electrons trapped at the NPs' surfaces.<sup>50</sup> Similar to our observations, the bleaching of the sub-band-gap light induced by above-band-gap excitation was also recently observed in other wide-band-gap semiconductor NWs [i.e., GaN,<sup>51,52</sup>  $\text{In}_2\text{O}_3$ ,<sup>53</sup> and  $\text{SnO}_2$  (Ref. 54) NWs]—prepared by thermal evaporation methods, which was attributed to the state-filling effect of the sub-band-gap defect states. We believe that the contrasting results are due to the different absorption cross sections and location of the defect energy levels in ZnO nanostructures prepared by different methods. Complementary  $z$ -scan measurements were therefore also conducted to verify the observed  $\Delta T/T$  results. The  $z$ -scan measurements of these NW samples at 470 nm showed an increase in transmittance (i.e., a saturable absorption) in contrast to a decrease in transmittance (i.e., reverse saturable absorption) for bulk ZnO (see Supplemental Material for the results of the  $z$ -scan measurements for ZnO NWs and single-crystal bulk ZnO<sup>34</sup>). This is attributed to the larger ground-state absorption cross section of the defect states compared to its excited-state absorption cross section. The  $z$ -scan results confirm that the observed positive  $\Delta T/T$  of sub-band-gap light is due to the state-filling-induced absorption bleaching of the visible probe light rather than stimulated emission.

In the limit of a small change in transmittance with  $\Delta T/T \ll 1$ , the state-filling-induced transmission changes can be expressed as<sup>55</sup>

$$\Delta T/T \approx -\Delta\alpha(\hbar\omega)d = \sum_i (n_i^e + n_i^h)\alpha_{0,i}(\hbar\omega)d, \quad (1)$$

where  $\alpha_{0,i}(\hbar\omega)$  is the contribution of transition  $\hbar\omega_i$  to the ground-state absorption at the probe wavelength,  $n_i^e$  ( $n_i^h$ ) are occupation numbers of the electron (hole) states involved in the transition, and  $d$  is the thickness of the sample. State filling of either the hole or electron states results in a decrease in absorption or an increase in transmission. Therefore,

under the conditions of the same excitation fluence and equivalent sample thicknesses, the relative magnitude of the state-filling-induced absorption bleaching (at a specific probe wavelength) compared to the DT spectra is reflective of the magnitude of the ground-state absorption  $\alpha_0$  of the defects states in the band gap. Its magnitude is also a measure of the relative population (or concentration) of the GE centers—with the air-annealed sample possessing the largest concentration of GE centers. This is nonetheless consistent with the relative GE intensities from the different samples in Fig. 2(a). Hence, the occupancy of the photoexcited electrons in the CB ( $n^e$ ) and holes trapped in the GE-related deep levels ( $n^h$ ) are monitored, as illustrated by a schematic in the inset of Fig. 3(b).

The GE peak exhibits an energy redshift of  $\sim 180$  meV relative to the PB peak (at  $\sim 2.64$  eV or  $\sim 470$  nm) as shown in Fig. 3. We attribute this redshift to the energy difference between the level interrogated by the probe beam and the CB band-edge and/or shallow donor level (i.e., whose electrons are involved in the GE)—see Fig. 4(b).<sup>56</sup> The probe is sensitive to the hot electrons relaxing down to the CBM/shallow donor level and the holes in the GE centers; therefore the PB arises due to the state filling of the electrons/holes at these energy levels. The broad PB peak spanning from 450 to 600 nm is likely due to the broad distribution of the energy levels of the GE centers monitored by the probe. From the PB peak, the energy level of the GE centers is located at  $\sim 0.88$  eV ( $=E_g + 0.18$  eV  $- 2.64$  eV) above the VBM, which agrees well with the

calculated  $\varepsilon(+/0)$  transition level of  $V_{ZnO}$  (i.e.,  $\sim 0.6$ – $0.8$  eV above the VBM) published in a recent density functional study.<sup>30</sup> Previously, positron annihilation spectroscopy (PAS) of pressurized melt-grown single-crystal ZnO and theoretical calculations revealed that  $V_{ZnO}$  exists in a neutral state and is present in high concentrations ( $\sim 10^{17}$  cm<sup>-3</sup>).<sup>57</sup> Therefore, the neutral  $V_{ZnO}$  (or  $V_{ZnO}^0$ ) can be one of the more likely candidates of the source of GE.

#### D. Excitonic Auger-type ultrafast hole trapping to the GE centers

Next we turn our attention to examine the dynamics of the hole trapping to these GE centers. From the buildup time of the PB peak at the 470-nm probe wavelength, the nature of this hole trapping process could be validated in a pump-fluence-dependent study. Given that the probe is resonant with the state filling of the GE centers and the CBM, the buildup time from the DT spectra is in fact a convolution of the signals from the interband trapping of the holes from the VB to the GE centers and those from the electrons undergoing fast intraband relaxation to the CBM from higher levels in the CB. The intraband relaxation rate of the photoexcited electrons in the CB is dependent on the amount of excess energy above the CBM and the carrier densities, which should be almost comparable in these samples under the same excitation conditions. This intraband electron relaxation is expected to be extremely fast [e.g., occurring at less than 30 fs for electron energies greater than 0.1 eV above the CBM at the ZnO (10 $\bar{1}0$ ) surface<sup>58</sup>]. Hence, the buildup dynamics measured here is clearly dominated by the interband hole trapping process from the ZnO host to the GE centers.

Figure 4(a) shows the normalized DT transients of the PB buildup for the as-grown, air-annealed, and H<sub>2</sub>-annealed ZnO NWs at 470-nm probe wavelength, where the best-fit rise times  $\tau_{rise}$  are  $\sim 370 \pm 20$  fs,  $180 \pm 10$  fs, and  $450 \pm 20$  fs, respectively. Interestingly, the rise time is the slowest for the H<sub>2</sub>-annealed sample, while it is the fastest for the air-annealed sample. As the buildup time is dominated by the hole trapping process to the GE centers, the variation in  $\tau_{rise}$  is therefore attributed to the different concentrations of the GE centers present in these three samples. Since the hole trapping rate is determined by the expression  $\tau_h^{-1} = c_p N_{GE}$ ,<sup>59</sup> where  $c_p$  (cm<sup>3</sup>/s) is the hole-capture coefficient, the higher the concentration of the GE centers, the faster is the hole trapping time ( $\tau_h$ ). The capture cross section of the photoexcited holes can be calculated:  $\sigma_h = (\tau_h v_{th} N_{GE})^{-1}$ , where  $v_{th}$  is the hole thermal velocity  $\sim 10^7$  cm/s, and  $N_{GE}$  is the concentration of GE centers. Due to the fast hole trapping times,  $\sigma_h$  would be quite large. Though we could not directly measure  $N_{GE}$  in our samples, suppose  $N_{GE}$  is in the order of  $\sim 10^{17}$  cm<sup>-3</sup>, i.e., typical for as-grown ZnO bulk;<sup>57</sup>  $\sigma_h$  will be as large as  $\sim 10^{-12}$  cm<sup>2</sup>. This value is comparable to the hole capture cross section of deep hole traps in ZnO thin films.<sup>60</sup>

Generally, free carriers can be trapped by deep centers in semiconductors via one of the following mechanisms: multiphonon emission,<sup>61</sup> phonon-assisted cascade capture process,<sup>62</sup> or Auger recombination processes (classical vs excitonic).<sup>63,64</sup> However, the extremely fast  $\tau_h$  uncovered by TAS strongly suggests that the energy loss is dominated by

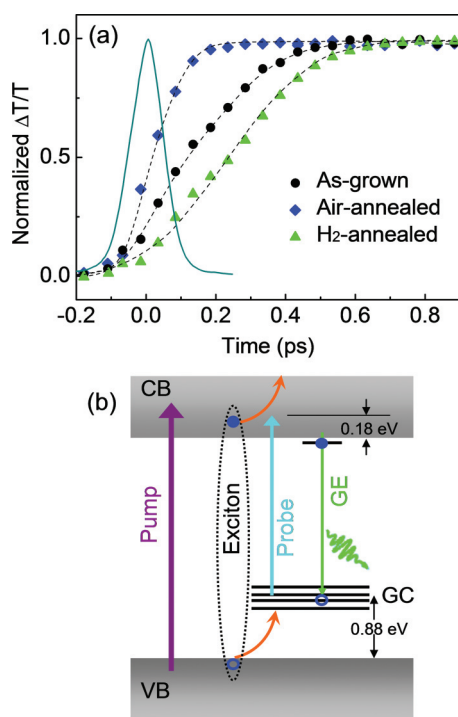


FIG. 4. (Color online) (a) Normalized  $\Delta T/T$  transients of the photobleaching (PB) buildup for the as-grown, air-annealed and H<sub>2</sub>-annealed ZnO NWs at 470-nm probe wavelength. The pump wavelength used was 350 nm and the pump fluence was  $50 \mu\text{J}/\text{cm}^2$ . The solid line is the system response and the dashed lines are the fitting curves with the system response deconvoluted; (b) a schematic of the proposed excitonic Auger-type ultrafast hole trapping at the GE centers. (GC) GE centers.

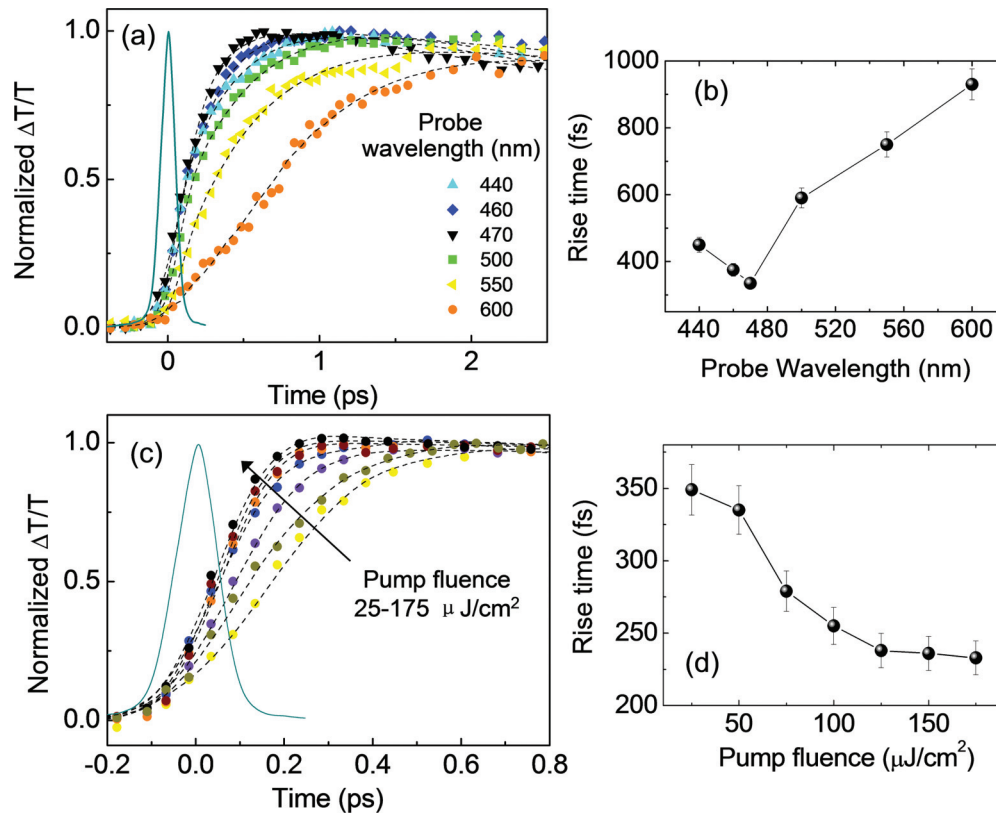


FIG. 5. (Color online) (a) Normalized  $\Delta T/T$  transients of the as-grown ZnO NW sample as a function of probe wavelengths; (b) the fitted rise time as a function of probe wavelength; (c) normalized  $\Delta T/T$  transients of the as-grown ZnO NW sample as a function of pump fluence at 470 nm; (d) the fitted rise time as a function of pump fluence. The solid line in (a) and (c) is the system response and the dashed lines are the fitting curves with the system response deconvolved. The pump wavelength used was 350 nm.

a non-phonon mechanism. Given the large energy separation between the GE center and the VBM ( $\sim 1$  eV) and the ultrafast hole trapping lifetimes ( $\tau_h \sim$ hundreds of fs), the calculated energy-loss rate of 1.6–2.7 eV/ps is many orders of magnitude greater than the relaxation rate expected for the multiphonon emission and the cascade capture process.<sup>65,66</sup> The classical Auger recombination requires two independent free carriers to be located at the impurity site and hence is expected to be inefficient. On the other hand, the excitonic Auger capture mechanism as proposed by Hangleiter is more likely.<sup>64,67</sup> It is because the large extension of the exciton wave function in  $\kappa$  space can lead to an increase in the excitonic Auger transition probability  $W$  [ $W \sim \alpha_0^{-3}$ ,<sup>67</sup> where  $\alpha_0$  is the exciton Bohr radius and in ZnO, the free exciton Bohr radius of ZnO is very small ( $\sim 1.8$  nm)]. Following above-band-gap photoexcitation, free excitons are formed in ZnO. When a free exciton meets the GE center, its hole can be captured by the GE center while its electron is excited to higher energy levels in the CB, taking with it the excess energy—see Fig. 4(b). These electrons in the higher energy levels subsequently relax back to the CBM via phonon emission.

Probe wavelength and pump-fluence-dependent DT were also performed on the as-grown sample to further investigate the hole trapping dynamics. Figure 5(a) shows the buildup dynamics at probe wavelengths from 440 to 600 nm. Figure 5(b) shows the fitted rise times which vary from  $340 \pm 20$  fs to  $950 \pm 50$  fs, where  $\tau_h$  is fastest at the peak of the PB band

( $\sim 470$  nm). The broad PB peak spanning from 450 to 600 nm is likely due to the broad distribution of the energy levels of the GE centers monitored by the probe. The longer wavelengths correspond to the higher energy levels of the GE centers with respect to the VBM as shown in Fig. 4(b). Therefore the different rise times for the different probe wavelengths reflect the various hole trapping times to the different energy levels of the GE centers. Consistent with our above results where a sample with a higher concentration of GE centers exhibits a faster hole trapping rate ( $\tau_h^{-1} = c_p N_{\text{GE}}$ ), it is interpreted that  $\tau_h$  is dependent on the density of states (DOS) distribution of GE centers where the energy levels with a shorter  $\tau_h$  possess a higher DOS. Therefore, away from the DOS maximal (i.e., near the PB peak position), the PB signal decreases as shown in Fig. 3(b) and  $\tau_h$  becomes slower.

Lastly, Fig. 5(c) shows the buildup dynamics as a function of increasing pump fluence. Figure 5(d) shows the fitted rise times which shorten from  $350 \pm 20$  fs to  $250 \pm 10$  fs with increasing pump fluence. This behavior is consistent with the excitonic Auger-type mechanism where increasing free exciton concentrations result in an increase in the hole capture coefficients—hence the shortening of the hole trapping lifetimes.<sup>67</sup> The excitonic Auger-like mechanism could therefore account for the ultrafast sub-ps hole trapping times to the GE center, thus validating our earlier hypothesis.

Based on the above results, we propose that  $V_{\text{ZnO}}^0$  divacancies on/near the ZnO (10 $\bar{1}$ 0) surface can be one of the

most likely candidates of the GE centers in our VPT-prepared ZnO NWs. The photoexcited holes in the VB are subsequently trapped at  $V_{\text{ZnO}}^0$  by an excitonic Auger-like process on an ultrafast (hundreds of femtoseconds) time scale (i.e.,  $V_{\text{ZnO}}^0 + h^+ \rightarrow V_{\text{ZnO}}^+$ ). The resultant  $\varepsilon(+/0)$  charge transition from CB to  $V_{\text{ZnO}}^+$  then gives rise to the GE (i.e.,  $V_{\text{ZnO}}^+ + e \rightarrow V_{\text{ZnO}}^0 + h\nu_{\text{GE}}$ ). Charge separation of the photogenerated electron-hole pairs by this ultrafast hole trapping mechanism will suppress the BE emission at low pump fluence. This was indeed observed for a low pump fluence of  $\sim 0.5 \mu\text{J}/\text{cm}^2$  (see Fig. S5 in the Supplemental Material<sup>34</sup>)—consistent with the reports of VPT-grown ZnO NWs.<sup>68</sup> These trapped holes on the ZnO NW surfaces with long ( $\mu\text{s}$ ) recombination lifetimes are highly beneficial for the oxidative processes in a photocatalytic reaction. Our findings could therefore account for the enhanced photocatalytic activities in oxidative reactions at the ZnO (10 $\bar{1}0$ ) surface,<sup>69</sup> and in the VPT-fabricated ZnO nanostructures with strong GE intensities.<sup>6,29</sup>

#### IV. CONCLUSIONS

In conclusion, a comprehensive ultrafast optical spectroscopy study on the origin of GE and charge trapping dynamics was performed on undoped as-grown, air-annealed, and H<sub>2</sub>-annealed ZnO NWs fabricated by the VPT method. A sub-band-gap absorption bleaching band was observed in TAS upon above-band-gap photoexcitation, which is due to the

state filling of the electrons in the conduction band/shallow donor level and the holes trapped at the GE centers. The GE involves the transitions of the electrons in the CB and/or shallow (delocalized) donor levels with holes trapped at the GE centers that are located at 0.88 eV above the VBM. Importantly, an ultrafast excitonic Auger-type hole trapping process to the GE centers occurring in a sub-ps timescale was uncovered by TAS, which is strongly dependent on the concentration of GE centers, the DOS of energy levels of the GE centers, and also the free exciton densities. Our findings shed new light on the ultrafast charge trapping mechanism in ZnO NWs, which has strong implications for the development of ZnO-based photocatalytic and optoelectronic devices.

#### ACKNOWLEDGMENTS

This work is supported by the following research grants: NTU start-up Grant No. M4080514.110 NTU (M58110068), Academic Research Fund (AcRF) Tier 1 Grant No. M4010802.110 RG49/08 (M52110082), a Ministry of Education AcRF Tier 2 Grant No. MOE2011-T2-2-051 (M402110000), and a Competitive Research Programme (CRP) grant under Project No. NRF-CRP5-2009-04. G.X. and T.C.S. also acknowledge funding support from the Singapore National Research Foundation (NRF) through the Singapore-Berkeley Research Initiative for Sustainable Energy (SinBeRISE) CREATE Programme.

\*Corresponding author: tzechien@ntu.edu.sg

- <sup>1</sup>C. Jagadish and S. J. Pearton, *Zinc Oxide Bulk, Thin Films and Nanostructures: Processing, Properties and Applications* (Elsevier, Amsterdam, Boston, 2006).
- <sup>2</sup>C. H. Chuang and C. Burda, *J. Phys. Chem. Lett.* **3**, 1921 (2012).
- <sup>3</sup>M. Kong, Y. Z. Li, X. Chen, T. T. Tian, P. F. Fang, F. Zheng, and X. J. Zhao, *J. Am. Chem. Soc.* **133**, 16414 (2011).
- <sup>4</sup>Y. F. Hsu, Y. Y. Xi, A. B. Djurisić, and W. K. Chan, *Appl. Phys. Lett.* **92**, 133507 (2008).
- <sup>5</sup>Q. Wan, T. H. Wang, and J. C. Zhao, *Appl. Phys. Lett.* **87**, 083105 (2005).
- <sup>6</sup>Y. H. Zheng, L. R. Zheng, Y. Y. Zhan, X. Y. Lin, Q. Zheng, and K. M. Wei, *Inorg. Chem.* **46**, 6980 (2007).
- <sup>7</sup>T. J. Kuo, C. N. Lin, C. L. Kuo, and M. H. Huang, *Chem. Mater.* **19**, 5143 (2007).
- <sup>8</sup>D. Li, Y. H. Leung, A. B. Djurišić, Z. T. Liu, M. H. Xie, S. L. Shi, S. J. Xu, and W. K. Chan, *Appl. Phys. Lett.* **85**, 1601 (2004).
- <sup>9</sup>U. Pal and P. Santiago, *J. Phys. Chem. B* **109**, 15317 (2005).
- <sup>10</sup>E. De la Rosa, S. Sepulveda-Guzman, B. Reesja-Jayan, A. Torres, P. Salas, N. Elizondo, and M. J. Yacamán, *J. Phys. Chem. C* **111**, 8489 (2007).
- <sup>11</sup>S. J. Lee, S. K. Park, C. R. Park, J. Y. Lee, J. Park, and Y. R. Do, *J. Phys. Chem. C* **111**, 11793 (2007).
- <sup>12</sup>M. H. Huang, S. Mao, H. Feick, H. Q. Yan, Y. Y. Wu, H. Kind, E. Weber, R. Russo, and P. D. Yang, *Science* **292**, 1897 (2001).
- <sup>13</sup>P. J. Pauzauskis and P. Yang, *Mater. Today* **9**, 36 (2006).
- <sup>14</sup>A. B. Djurišić, W. C. H. Choy, V. A. L. Roy, Y. H. Leung, C. Y. Kwong, K. W. Cheah, T. K. Gundu Rao, W. K. Chan, H. F. Lui, and C. Surya, *Adv. Funct. Mater.* **14**, 856 (2004).

- <sup>15</sup>H. Z. Xue, N. Pan, R. G. Zeng, M. Li, X. Sun, Z. J. Ding, X. P. Wang, and J. G. Hou, *J. Phys. Chem. C* **113**, 12715 (2009).
- <sup>16</sup>N. Pan, X. P. Wang, M. Li, F. Q. Li, and J. G. Hou, *J. Phys. Chem. C* **111**, 17265 (2007).
- <sup>17</sup>J. P. Richters, T. Voss, L. Wischmeier, I. Ruckmann, and J. Gutowski, *Appl. Phys. Lett.* **92**, 011103 (2008).
- <sup>18</sup>R. Dingle, *Phys. Rev. Lett.* **23**, 579 (1969).
- <sup>19</sup>K. Vanheusden, W. L. Warren, C. H. Seager, D. R. Tallant, J. A. Voigt, and B. E. Gnade, *J. Appl. Phys.* **79**, 7983 (1996).
- <sup>20</sup>A. van Dijken, E. A. Meulenkaamp, D. Vanmaekelbergh, and A. Meijerink, *J. Phys. Chem. B* **104**, 1715 (2000).
- <sup>21</sup>A. Janotti and C. G. Van de Walle, *Phys. Rev. B* **76**, 165202 (2007).
- <sup>22</sup>B. X. Lin, Z. X. Fu, and Y. B. Jia, *Appl. Phys. Lett.* **79**, 943 (2001).
- <sup>23</sup>P. S. Xu, Y. M. Sun, C. S. Shi, F. Q. Xu, and H. B. Pan, *Nucl. Instrum. Methods Phys. Res., Sect. B* **199**, 286 (2003).
- <sup>24</sup>N. O. Korsunskaya, L. V. Borkovskaya, B. M. Bulakh, L. Y. Khomenkova, V. I. Kushnirenko, and I. V. Markevich, *J. Lumin.* **102**, 733 (2003).
- <sup>25</sup>R. Vidya, P. Ravindran, H. Fjellvag, B. G. Svensson, E. Monakhov, M. Ganchenkova, and R. M. Nieminen, *Phys. Rev. B* **83**, 045206 (2011).
- <sup>26</sup>M. J. Li, G. C. Xing, L. F. N. A. Qune, G. Z. Xing, T. Wu, C. H. A. Huan, X. H. Zhang, and T. C. Sum, *Phys. Chem. Chem. Phys.* **14**, 3075 (2012).
- <sup>27</sup>H. Kaftelen, K. Ocakoglu, R. Thomann, S. Tu, S. Weber, and E. Erdem, *Phys. Rev. B* **86**, 014113 (2012).
- <sup>28</sup>X. J. Wang, L. S. Vlasenko, S. J. Pearton, W. M. Chen, and I. A. Buyanova, *J. Phys. D: Appl. Phys.* **42**, 175411 (2009).

- <sup>29</sup>A. J. Morfa, B. C. Gibson, M. Karg, T. J. Karle, A. D. Greentree, P. Mulvaney, and S. Tomljenovic-Hanic, *Nano Lett.* **12**, 949 (2012).
- <sup>30</sup>A. Chakrabarty and C. H. Patterson, *J. Chem. Phys.* **137**, 054709 (2012).
- <sup>31</sup>R. Kovacic, B. Meyer, and D. Marx, *Angew. Chem., Int. Ed.* **46**, 4894 (2007).
- <sup>32</sup>R. P. Prasankumar, P. C. Upadhyaya, and A. J. Taylor, *Phys. Status Solidi B* **246**, 1973 (2009).
- <sup>33</sup>M. H. Huang, Y. Y. Wu, H. Feick, N. Tran, E. Weber, and P. D. Yang, *Adv. Mater.* **13**, 113 (2001).
- <sup>34</sup>See Supplemental Material at <http://link.aps.org/supplemental/10.1103/PhysRevB.87.115309> for detailed results of the SEM images of air-annealed and H<sub>2</sub>-annealed ZnO NWs, TRPL of GE in as-grown and Cu-doped ZnO NWs, *z*-scan measurements for ZnO NWs and single-crystal bulk ZnO, and the PL spectrum of the ZnO NWs excited at low pump fluence.
- <sup>35</sup>D. Wang, H. W. Seo, C. C. Tin, M. J. Bozack, J. R. Williams, M. Park, N. Sathitsuksanoh, A. J. Cheng, and Y. H. Tzeng, *J. Appl. Phys.* **99**, 113509 (2006).
- <sup>36</sup>X. Q. Meng, D. X. Zhao, J. Y. Zhang, D. Z. Shen, Y. M. Lu, L. Dong, Z. Y. Xiao, Y. C. Liu, and X. W. Fan, *Chem. Phys. Lett.* **413**, 450 (2005).
- <sup>37</sup>A. Dev, R. Niepelt, J. P. Richters, C. Ronning, and T. Voss, *Nanotechnology* **21**, 065709 (2010).
- <sup>38</sup>E. V. Lavrov, J. Weber, F. Borner, C. G. Van de Walle, and R. Helbig, *Phys. Rev. B* **66**, 165205 (2002).
- <sup>39</sup>D. C. Reynolds, D. C. Look, B. Jogai, J. E. Van Nostrand, R. Jones, and J. Jenny, *Solid State Commun.* **106**, 701 (1998).
- <sup>40</sup>M. A. Reshchikov, F. Shahedipour, R. Y. Korotkov, B. W. Wessels, and M. P. Ulmer, *J. Appl. Phys.* **87**, 3351 (2000).
- <sup>41</sup>F. J. Xu, B. Shen, L. Lu, Z. L. Miao, J. Song, Z. J. Yang, G. Y. Zhang, X. P. Hao, B. Y. Wang, X. Q. Shen, and H. Okumura, *J. Appl. Phys.* **107**, 023528 (2010).
- <sup>42</sup>G. Z. Xing, YH Lu, Y. F. Tian, J. B. Yi, C. C. Lim, Y. F. Li, G. P. Li, D. D. Wang, B. Yao, J. Ding, Y. P. Feng, and T. Wu, *AIP Adv.* **1**, 022152 (2011).
- <sup>43</sup>Z. P. Wei, D. L. Guo, B. Liu, R. Chen, L. M. Wong, W. F. Yang, S. J. Wang, H. D. Sun, and T. Wu, *Appl. Phys. Lett.* **96**, 031902 (2010).
- <sup>44</sup>D. C. Reynolds, D. C. Look, and B. Jogai, *J. Appl. Phys.* **89**, 6189 (2001).
- <sup>45</sup>G. Xing, G. Xing, M. Li, E. J. Sie, D. Wang, A. Sulistio, Q. Ye, C. H. A. Huan, T. Wu, and T. C. Sum, *Appl. Phys. Lett.* **98**, 102105 (2011).
- <sup>46</sup>R. Y. Korotkov, M. A. Reshchikov, and B. W. Wessels, *Physica B* **273–274**, 80 (1999).
- <sup>47</sup>M. A. Reshchikov, J. Q. Xie, B. Hertog, and A. Osinsky, *J. Appl. Phys.* **103**, 103514 (2008).
- <sup>48</sup>M. A. Reshchikov and H. Morkoc, *J. Appl. Phys.* **97**, 061301 (2005).
- <sup>49</sup>M. Schirra, R. Schneider, A. Reiser, G. M. Prinz, M. Feneberg, J. Biskupek, U. Kaiser, C. E. Krill, K. Thonke, and R. Sauer, *Phys. Rev. B* **77**, 125215 (2008).
- <sup>50</sup>J. J. Cavaleri, D. E. Skinner, D. P. Colombo, and R. M. Bowman, *J. Chem. Phys.* **103**, 5378 (1995).
- <sup>51</sup>P. C. Upadhyaya, Q. M. Li, G. T. Wang, A. J. Fischer, A. J. Taylor, and R. P. Prasankumar, *Semicond. Sci. Technol.* **25**, 024017 (2010).
- <sup>52</sup>D. Tsokkou, A. Othonos, and M. Zervos, *J. Appl. Phys.* **106**, 054311 (2009).
- <sup>53</sup>D. Tsokkou, A. Othonos, and M. Zervos, *J. Appl. Phys.* **106**, 084307 (2009).
- <sup>54</sup>A. Othonos, M. Zervos, and D. Tsokkou, *Nanoscale Res. Lett.* **4**, 828 (2009).
- <sup>55</sup>V. I. Klimov, *Semiconductor and Metal Nanocrystals. Synthesis and Electronic and Optical Properties* (Dekker, New York, 2004).
- <sup>56</sup>V. I. Klimov and D. W. McBranch, *Phys. Rev. B* **55**, 13173 (1997).
- <sup>57</sup>G. Brauer, W. Anwand, W. Skorupa, J. Kuriplach, O. Melikhova, C. Moisson, H. von Wenckstern, H. Schmidt, M. Lorenz, and M. Grundmann, *Phys. Rev. B* **74**, 045208 (2006).
- <sup>58</sup>W. A. Tisdale, M. Muntwiler, D. J. Norris, E. S. Aydil, and X. Y. Zhu, *J. Phys. Chem. C* **112**, 14682 (2008).
- <sup>59</sup>A. Hangleiter, *Phys. Rev. B* **35**, 9149 (1987).
- <sup>60</sup>M. Schmidt, H. von Wenckstern, R. Pickenhain, and M. Grundmann, *Solid State Electron.* **75**, 48 (2012).
- <sup>61</sup>T. N. Morgan, *Phys. Rev. B* **28**, 7141 (1983).
- <sup>62</sup>M. Lax, *Phys. Rev.* **119**, 1502 (1960).
- <sup>63</sup>A. Haug, *J. Phys. Chem. Solids* **49**, 599 (1988).
- <sup>64</sup>S. Rein, *Lifetime Spectroscopy—A Method of Defect Characterization in Silicon for Photovoltaic Applications* (Springer, Berlin, 2005).
- <sup>65</sup>T. Inoshita and H. Sakaki, *Phys. Rev. B* **46**, 7260 (1992).
- <sup>66</sup>V. I. Klimov, *J. Phys. Chem. B* **104**, 6112 (2000).
- <sup>67</sup>A. Hangleiter, *Phys. Rev. B* **37**, 2594 (1988).
- <sup>68</sup>J. C. Johnson, H. Q. Yan, P. D. Yang, and R. J. Saykally, *J. Phys. Chem. B* **107**, 8816 (2003).
- <sup>69</sup>N. Kislov, J. Lahiri, H. Verma, D. Y. Goswami, E. Stefanakos, and M. Batzill, *Langmuir* **25**, 3310 (2009).